Tomographic diffractive microscopy with a wavefront sensor

Y. Ruan,[1] P. Bon,[1,2] E. Mudry,[1] G. Maire,[1,*] P. C. Chaumet,[1] H. Giovannini,[1] K. Belkebir,[1] A. Talneau,[3] B. Wattellier,[2] S. Monneret,[1] and A. Sentenac[1]

[1]*Institut Fresnel, CNRS, Aix-Marseille Université, Ecole Centrale Marseille, Campus de St. Jérôme, 13013 Marseille, France*

[2]*PHASICS SA, XTEC Bt. 404, Campus de l'Ecole Polytechnique, Route de Saclay, 91128 Palaiseau, France*

[3]*Laboratoire de Photonique et de Nanostructures, 91460 Marcoussis, France*

**Corresponding author: guillaume.maire@fresnel.fr*

Received January 12, 2012; accepted January 26, 2012;
posted January 31, 2012 (Doc. ID 161421); published May 7, 2012

Tomographic diffractive microscopy is a recent imaging technique that reconstructs quantitatively the three-dimensional permittivity map of a sample with a resolution better than that of conventional wide-field microscopy. Its main drawbacks lie in the complexity of the setup and in the slowness of the image recording as both the amplitude and the phase of the field scattered by the sample need to be measured for hundreds of successive illumination angles. In this Letter, we show that, using a wavefront sensor, tomographic diffractive microscopy can be implemented easily on a conventional microscope. Moreover, the number of illuminations can be dramatically decreased if a constrained reconstruction algorithm is used to recover the sample map of permittivity. © 2012 Optical Society of America

OCIS codes: 180.6900, 110.1758.

Tomographic diffractive microscopy (TDM) has recently emerged as a powerful imaging technique for retrieving the three-dimensional (3D) map of permittivity of unstained samples [1,2] with high resolution. It consists in recording hundreds of holograms of the probed object under various illumination angles and processing these data with an inversion algorithm to estimate the object permittivity map. This technique has been successfully applied to biological samples, where the permittivity contrast is weak and linear approximations (such as the Born approximation) can be used to model the link between the holograms and the permittivity [3–6]. In this case, the permittivity map can be retrieved by Fourier transforming the data. Axial and transverse resolutions about twice better than that of wide-field and confocal microscopy have been observed with this approach [2].

Although the theoretically and experimentally observed performances of TDM make it a very promising imaging technique for nonfluorescent samples, its development remains hindered by the complexity and slowness of its practical implementation. The necessity to measure both the phase and the amplitude of the scattered field is generally accomplished by adding a reference beam to the setup and recording an interference pattern in an on-axis or an off-axis arrangement [2]. This approach, which requires the use of light sources with high temporal coherence, is plagued by the speckle noise stemming from the parasitic reflections and scattering along the light path. The phase-stepping methods in the on-axis technique are generally time consuming and very sensitive to stability perturbations, whereas the off-axis technique imposes additional constraints on the data discretization. Since hundreds of holograms under different illumination angles are typically required to reconstruct the 3D permittivity map of the samples with the usual Fourier-transform-based inversion algorithms [3–5], the experimental difficulty (especially concerning the stability of the interferometric module) and the recording time of TDM are significantly increased.

To ameliorate the practical performances of TDM, a high-speed setup [5] and a common path interferometer geometry [6] have been reported, but these solutions cannot be readily implemented in a standard microscope. In this Letter, we show that it is possible to accelerate dramatically the TDM image recording while simplifying its adaptation to any standard microscope by using a wavefront sensor and an efficient inversion algorithm.

Our TDM setup is based on a reflection microscope, as seen in Fig. 1, in which the camera has been replaced by a wavefront sensor. A collimated laser beam (He–Ne, $\lambda = 633$ nm), controlled by a mirror mounted on step motors (Newport NSA12), illuminates the sample through an objective with NA = 0.95 (Zeiss Epiplan-Apochromat 50×) under various angles of incidence. The backscattered field is imaged with a 290× magnification on a high-resolution wavefront sensor (Phasics SID4-HR, 400 × 300 pixels) based on quadriwave lateral shearing interferometry [7]. No reference path is needed, and both the phase and the intensity of the imaged field are retrieved with a single shot measurement. To demonstrate the potential of our setup for reconstructing the permittivity map of 3D samples, we consider a test object made of four resin cylinders deposited on a reflective silicon substrate. The cylinders have a diameter close

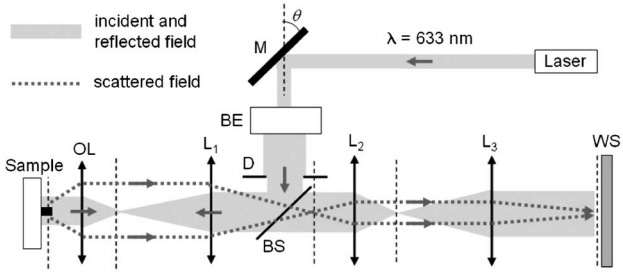

Fig. 1. Schematic of the TDM setup. M, rotative mirror; BE, beam expander; D, diaphragm; BS, beam splitter; OL, objective lens; L1, tube lens; L2, L3, relay lenses ($f' = 3.5$ and 20 cm); WS, wavefront sensor.

to 1 μm, a height of 120 nm, and their axes are placed at the corners of a square with 2 μm side.

Generally, wavefront sensors are used to estimate slow phase variations like those produced by aberrations of lenses or weakly scattering biological samples. At $\lambda = 633$ nm, our wavefront sensor can detect a phase difference between two adjacent pixels from 0.01 to 2.9 rad [7]. The constraint imposed by this upper bound is greatly relaxed by sampling the point spread function of the setup with about eight pixels (105 nm per pixel with the magnification). To verify that the sensor is able to recover quantitatively the phase and amplitude scattered by our relatively contrasted samples, we compared, for the same successive illumination angles, its image fields to those given by on-axis phase-shifting interferometry with a standard CCD camera. For the wavefront sensor, a phase reference is measured on the bare substrate for each illumination prior to imaging the sample, and single shot measurements are performed. This reference further diminishes speckle noise that is already greatly reduced by the multi-illumination measurement. For phase-shifting interferometry, 30 images are averaged for each illumination to increase the signal-to-noise ratio. We have used six illuminations in the plane (x,z) with the electric field orthogonal to the plane of incidence and six illuminations in the plane (y,z) with the electric field parallel to the plane of incidence, with polar angles varying in the [−30,30] deg range. Figure 2 shows a comparison of the phase and amplitude of the scattered far field within the objective NA for both techniques, obtained by Fourier transforming the measured image fields. The data have been restricted to about 2000 scattering angles centered on the specular reflection on the substrate. The missing circle in the data corresponds to the domain where the field scattered by the sample is masked by this reflection. A very good agreement has been obtained between the two measurement methods for the whole data set.

To reconstruct the permittivity map of the sample, most reconstruction procedures assume that the far field

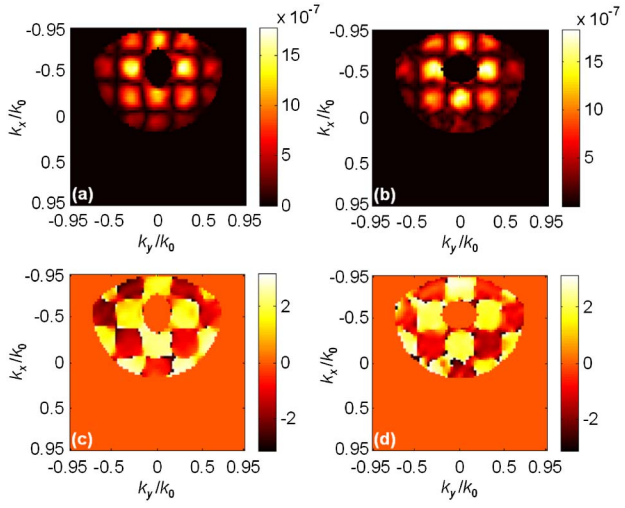

Fig. 2. (Color online) (a), (c) Wavefront sensor, amplitude, and phase of the scattered far field (30° illumination angle); (b), (d) same data for phase-shifting interferometry. k_x and k_y, spatial frequencies; k_0, wavenumber.

scattered in the $\mathbf{k}_d$ direction by an object illuminated by a plane wave with wave vector $\mathbf{k}_i$ is proportional to the Fourier transform of the relative permittivity contrast χ of the object [1,3,5,6] taken at $(\mathbf{k}_d - \mathbf{k}_i)$. For each illumination, the measured scattered field gives access to the Fourier components of the permittivity on a cap of sphere centered about $\mathbf{k}_i$ [2]. Changing the illumination angle permits us to explore another Fourier domain. Thus, the permittivity map can be simply retrieved by Fourier transforming the whole data set. This approach, valid for weakly contrasted samples, typically requires hundreds of illuminations to fill the whole accessible Fourier domain with fine enough discretization steps for the Fourier transform to be accurate.

In our configuration, the sample is deposited on a reflective substrate (for improving the axial resolution [8]), and the permittivity contrast of the resin in the air, close to 1, is higher than the ones usually met in biological samples (≤0.1). To image the sample with a limited number of views and to account for the substrate and the possible multiple scattering phenomenon, we have developed an iterative inversion technique based on a rigorous vectorial modeling of the wave–sample interaction. This algorithm has already been applied with success to the imaging of highly contrasted two-dimensional objects [9–11]. The inversion problem consists in retrieving the unknown relative permittivity contrast χ inside an investigation domain W from the measurements $\mathbf{f}_l$, with $l = 1,\ldots,\mathrm{L}$, of the scattered field in the far-field domain Γ obtained for L different illuminations. It relies on the relationship between χ and the scattered far field $\mathbf{E}_l^d$, which involves the total field that is formed inside the sample, $\mathbf{E}_l$ [12]. The latter reads in operator notation,

$$\mathbf{E}_l = \mathbf{E}_l^0 + \underline{\underline{A}}\chi\mathbf{E}_l, \tag{1}$$

$$\mathbf{E}_l^d = \underline{\underline{B}}\chi\mathbf{E}_l, \tag{2}$$

where $\mathbf{E}_l^0$ is the reference field that would exist in W in the absence of the sample for the lth illumination, and $\underline{\underline{A}}_{i,\mathrm{j}}$ ($\underline{\underline{B}}_{i,\mathrm{k}}$) gives the field radiated at point j in W (k in Γ) by a dipole source placed at point i in W. Note that $\underline{\underline{A}}$ and $\underline{\underline{B}}$ account for the presence of the substrate. In our approach, both χ and $\mathbf{E}_l$ are estimated iteratively so as to minimize the cost functional,

$$\mathcal{F}(\chi,\mathbf{E}_l) = \mathrm{C}_\Gamma \sum_{l=1}^{\mathrm{L}} \|\mathbf{f}_l - \underline{\underline{B}}\chi\mathbf{E}_l\|_\Gamma^2 + \mathrm{C}_\mathrm{W} \sum_{l=1}^{\mathrm{L}} \|\mathbf{E}_l - \mathbf{E}_l^0 - \underline{\underline{A}}\chi\mathbf{E}_l\|_\mathrm{W}^2, \tag{3}$$

where C_Γ and C_W are normalization coefficients. The first term of $\mathcal{F}$ ensures that the field scattered by the estimated object will be close to the measurements, while the second term ensures that the estimated total field in W will satisfy Maxwell equations for the estimated value of χ [9]. The initial guesses for $\mathbf{E}_l$ and χ are obtained by backpropagating the measurements [12]. The inversion procedure is first applied to a large investigating domain W with a coarse meshing. Then W is downsized to a box

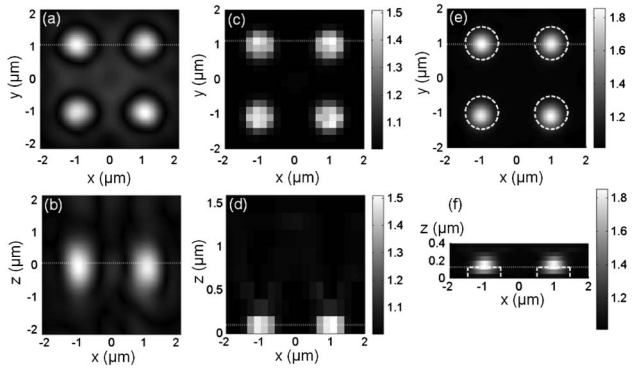

Fig. 3. Comparison of the modulus of the 3D inverse Fourier transform of the data set (53 nm meshing) [(a), (b)] and of the permittivity map retrieved with the iterative inversion algorithm [(c), (d), (e), (f)]. (c), (d) The height of the investigating domain is 1.6 μm with a mesh size of 200 nm. (e), (f) Zoom on the sample with a height of 0.4 μm and a mesh size of 50 nm (dashed white line, actual geometry of the sample). The figures in the top row show transverse cuts at (a), $z = 53$, (c) 100, and (e) 125 nm, and the ones in the bottom row longitudinal cuts at $y = 1$ μm. Cuts are along the white dotted lines.

adapted to the sample size, and the mesh is tightened for an improved resolution. Note that, in all our reconstructions, the absorption of the sample is neglected so that χ is sought as a positive real number.

Figure 3 compares the reconstructions, obtained from the wavefront sensor data, of the Fourier transform technique [Figs. 3(a) and 3(b), 53 nm meshing] and the iterative inversion procedure for different heights of W and different meshing: a height of 1.6 μm with 200 nm mesh size [Figs. 3(c) and 3(d)] and a height of 400 nm with 50 nm mesh size [Figs. 3(e) and 3(f)]. We observe that the Fourier transform technique provides a noisy reconstruction particularly distorted along the z axis. Indeed, the presence of the reflective surface is interpreted as a mirror object symmetrically placed along this axis. Moreover, this technique is very sensitive to the missing points in the Fourier space due to the restricted amount of data. Usually, several hundreds of illuminations are required to fill the Fourier space adequately. On the contrary, our reconstruction procedure estimates accurately the sample dimensions, even with the coarse meshing. Only four iterations were needed for the convergence of the iterative process, and similar reconstructions were obtained with the interferometric measurements. To our knowledge, this is the first time that such an iterative inversion procedure is successfully applied to 3D experimental data in optics. As only 12 illuminations were used, an acquisition time gain of more than 10 can be expected using our algorithm compared to the Fourier transform technique. On the other hand, as Eq. (1) has to be solved rigorously at each iteration, the computational time is significantly increased. Yet this rigorous calculation of $\mathbf{E}_l$ in W is necessary only if the sample supports multiple scattering. If the Born approximation is valid, $\mathbf{E}_l$ can be replaced by $\mathbf{E}_l^0$, and the computation time then remains comparable to that of the inverse Fourier transform.

In conclusion, the setup complexity and the long acquisition time of TDM can be dramatically ameliorated by using a wavefront sensor and constrained inversion procedures. With these improvements, TDM can be implemented in a conventional wide-field microscope, with low-cost weakly coherent sources, and the number of illuminations can be significantly reduced while retaining the high resolution and quantitative imaging performances of the technique.

The authors are very grateful to Laurent Milord for his contribution to the data treatment procedure.

References

1. V. Lauer, J. Microsc. **205**, 165 (2002).
2. O. Haeberlé, K. Belkebir, H. Giovannini, and A. Sentenac, J. Mod. Opt. **57**, 686 (2010).
3. M. Debailleul, B. Simon, V. Georges, O. Haeberlé, and V. Lauer, Meas. Sci. Technol. **19**, 074009 (2008).
4. Y. Sung, W. Choi, C. Fang-Yen, K. Badizadegan, R. R. Dasari, and M. S. Feld, Opt. Express **17**, 266 (2009).
5. M. Kim, Y. Choi, C. Fang-Yen, Y. Sung, R. Dasari, M. S. Feld, and W. Choi, Opt. Lett. **36**, 148 (2011).
6. R. Fiolka, K. Wicker, R. Heintzmann, and A. Stemmer, Opt. Express **17**, 12407 (2009).
7. P. Bon, G. Maucort, B. Wattellier, and S. Monneret, Opt. Express **17**, 13080 (2009).
8. E. Mudry, P. C. Chaumet, K. Belkebir, G. Maire, and A. Sentenac, Opt. Lett. **35**, 1857 (2010).
9. G. Maire, J. Girard, F. Drsek, H. Giovannini, A. Talneau, K. Belkebir, P. C. Chaumet, and A. Sentenac, J. Mod. Opt. **57**, 746 (2010).
10. G. Maire, F. Drsek, J. Girard, H. Giovannini, A. Talneau, D. Konan, K. Belkebir, P. C. Chaumet, and A. Sentenac, Phys. Rev. Lett. **102**, 213905 (2009).
11. J. Girard, G. Maire, H. Giovannini, A. Talneau, K. Belkebir, P. C. Chaumet, and A. Sentenac, Phys. Rev. A **82**, 061801(R) (2010).
12. K. Belkebir, P. C. Chaumet, and A. Sentenac, J. Opt. Soc. Am. A **22**, 1889 (2005).